

ORIGINAL ARTICLE

Small Ensemble-based Data Assimilation: A Machine Learning-Enhanced Data Assimilation Method with Limited Ensemble Size

Zhilin Li¹ | Yao Zhou¹ | Xianglong Li¹ | Zeng Liu² |
Zhaokuan Lu³ | Shanlin Xu⁴ | Seungnam Kim⁵ |
Guangyao Wang^{1,6,7}

¹Centre for Regional Oceans & Department of Ocean Science and Technology, Faculty of Science and Technology, University of Macau, Macau

²School of Naval Architecture and Ocean Engineering, Huazhong University of Science and Technology, Wuhan, Hubei, China

³Ningbo Institute of Dalian University of Technology, Ningbo, Zhejiang, China

⁴College of Civil Engineering, Zhejiang University of Technology, Hangzhou, Zhejiang, China

⁵Department of Naval Architecture and Ocean Engineering, Hongik University, Sejong, Republic of Korea

⁶State Key Laboratory of Internet of Things for Smart City, University of Macau, Macau

⁷Zhuhai UM Science and Technology Research Institute, Zhuhai, Guangdong, China

Correspondence
Guangyao Wang, PhD
Email: wanggy@um.edu.mo

Funding information
National Natural Science Foundation of China (52301336), Science and Technology Development Fund of Macau S.A.R. (0048/2025/ITP1), and University of Macau (SRG2025-00004-FST)

Ensemble-based data assimilation (DA) methods have become increasingly popular due to their inherent ability to address nonlinear dynamic problems. However, these methods often face a trade-off between analysis accuracy and computational efficiency, as larger ensemble sizes required for higher accuracy also lead to greater computational cost. In this study, we propose a novel machine learning-based data assimilation approach that combines the traditional ensemble Kalman filter (EnKF) with a fully connected neural network (FCNN). Specifically, our method uses a relatively small ensemble size to generate preliminary yet suboptimal analysis states via EnKF. A FCNN is then employed to learn and predict correction terms for these states, thereby mitigating the performance degradation induced by the limited ensemble size. We evaluate the performance of our proposed EnKF-FCNN method through numerical experiments involving Lorenz systems and nonlinear ocean wave field simulations. The results consistently demonstrate that the new method achieves higher accuracy than traditional EnKF with the same ensemble size, while incurring negligible additional computational cost. Moreover, the EnKF-FCNN method is adaptable to diverse applications through

coupling with different models and the use of alternative ensemble-based DA methods.

KEY WORDS

Data Assimilation, Machine Learning, Lorenz Systems, Ocean Wave

1 | INTRODUCTION

By solving a Bayesian estimation problem, data assimilation (DA) is a mathematical technique that combines model predictions and observations to obtain the optimal state estimate of dynamic systems [1]. Also, with the advancement of computation and observation technologies in the past few decades, DA methods have been commonly applied in various fields, such as meteorology [2, 3], physical oceanography [4, 5, 6], land surface processes [7, 8], and so on. With the inherent ability to describe the evolution of state error covariance, ensemble-based methods have become increasingly popular in addressing nonlinear problems, among which the ensemble Kalman filter (EnKF) is probably the most famous one with the non-intrusive nature and sequential DA capability [9, 10].

Despite their wide applications, ensemble-based DA methods are still facing one intractable problem, which is the trade-off between the analysis accuracy and computational efficiency [11, 12]. Specifically, a relatively large ensemble provides a better representation of the uncertainty, particularly the covariance matrices, leading to more accurate state estimations and vice versa. But it should be noted that the computational cost scales (almost) linearly with the ensemble size. Consequently, the computational burden can become unsustainable or impractical for high-dimensional nonlinear systems. Therefore, it is an inevitable problem to balance the desire for high accuracy with the practical limitations of available computational resources. From a statistical perspective, a limited ensemble size can lead to a rank-deficiency issue of the estimated covariance matrices, often resulting in spurious correlations and underestimation and eventually causing divergence. In this regard, two ad hoc methods have been developed to address the rank deficiency problem, i.e. localization [13] and inflation [14]. While these methods, along with their advanced variants, e.g. adaptive localization and inflation [15], can mitigate performance degradation induced by a limited ensemble size, substantial efforts are still required to optimize their configurations [16], which would inevitably increase the overall computational complexity.

The purpose of this paper is to show that the dilemma of ensemble-based DA methods can be significantly mitigated by machine learning (ML) methods, particularly neural networks (NNs). NNs are characterized by their ability to automatically learn and extract useful information from datasets, employing the composition of linear transformations with nonlinear activation functions to model complex relationships between inputs and outputs. Currently, NNs have shown potential to contribute to both the forecast and analysis steps involved in the DA-based simulations, although related research remains limited. In the forecast step, NNs are primarily used to build surrogate models that approximate the traditional, computationally expensive physical models, thereby accelerating the computational process [17, 18]. However, this approach can suffer from reduced accuracy and limited generalization ability when encountering new or extreme scenarios not well represented in the training dataset. Regarding the analysis step, NNs are mainly applied to learn the update process (e.g. EnKF formula) for handling missing or low-quality data [19, 20]. However, these methods rely on accurate estimates of covariance matrices, which typically depend on either a relatively large ensemble, ad hoc operations, or both.

In this study, we propose a novel small ensemble-based DA framework with machine learning, which can over-

come the systematic biases induced by a limited ensemble size effectively. Specifically, we develop the machine learning-enhanced DA framework on the basis of EnKF, initialized with a limited ensemble size. Then, a fully connected neural network (FCNN) is employed to learn a correction term for the analysis state, which is aimed at mitigating the suboptimal state estimation caused by the limited ensemble size. Consequently, the EnKF-FCNN coupled algorithm can offer both favorable computational efficiency and accuracy simultaneously. To evaluate the performance of the EnKF-FCNN coupled algorithm, we perform a set of numerical experiments based on the simulations of Lorenz systems (Lorenz-63 and Lorenz-96) and nonlinear ocean wave fields, which consistently demonstrate higher accuracy with negligible additional computational cost compared to traditional EnKF when using the same limited ensemble size. Moreover, the EnKF-FCNN method is highly adaptable across various applications by integrating with different models and employing alternative ensemble-based DA methods.

The paper is organized as follows. § 2 introduces the traditional EnKF and EnKF-FCNN coupled algorithms. The validation and benchmark of the EnKF-FCNN coupled algorithm based on the simulations of Lorenz systems and nonlinear ocean wave fields are presented in § 3. Finally, § 4 briefly summarizes this work.

2 | METHODS

2.1 | Ensemble Kalman filter

In this study, we use EnKF as the basis to develop the small ensemble-based DA method with machine learning, which basically includes the forecast and analysis steps as shown in Fig. 1. At the beginning time of the simulation $t = t_0$, an ensemble of initial conditions is first generated, usually based on the prescribed distribution information of measurements [4],

$$\mathbf{S}_{m,0} = \left[\mathbf{s}_{m,0}^{(1)}, \mathbf{s}_{m,0}^{(2)}, \dots, \mathbf{s}_{m,0}^{(n)}, \dots, \mathbf{s}_{m,0}^{(N-1)}, \mathbf{s}_{m,0}^{(N)} \right], \quad (1)$$

where \mathbf{s} represents the state vector and \mathbf{S} is the corresponding ensemble with size N and index $n = 1, 2, \dots, N$. Then with the forward model from time t_j to t_{j+1} , $\mathcal{M}_{j+1;j}$, the forecast step is performed by conducting N simulations (here $j = 0$)

$$\mathbf{s}_{f,1}^{(n)} = \mathcal{M}_{1:0}(\mathbf{s}_{m,0}^{(n)}), \quad (2)$$

which results in the ensemble of forecast results at $t = t_1$,

$$\mathbf{S}_{f,1} = \left[\mathbf{s}_{f,1}^{(1)}, \mathbf{s}_{f,1}^{(2)}, \dots, \mathbf{s}_{f,1}^{(n)}, \dots, \mathbf{s}_{f,1}^{(N-1)}, \mathbf{s}_{f,1}^{(N)} \right]. \quad (3)$$

Afterwards the analysis step is initialized by evaluating the forecast mean

$$\bar{\mathbf{s}}_{f,1} = \frac{1}{N} \sum_{n=1}^N \mathbf{s}_{f,1}^{(n)}, \quad (4)$$

and forecast error covariance matrix

$$\mathbf{P}_{f,1} = \mathcal{C}(\mathbf{S}_{f,1}), \quad (5)$$

where \mathcal{C} is a covariance operator defined as

$$\mathcal{C}(\mathbf{S}) = \frac{1}{N-1} \mathbf{S}'(\mathbf{S}')^\top, \quad (6)$$

$$\mathbf{S}' = [\mathbf{s}^{(1)} - \bar{s}, \mathbf{s}^{(2)} - \bar{s}, \dots, \mathbf{s}^{(n)} - \bar{s}, \dots, \mathbf{s}^{(N-1)} - \bar{s}, \mathbf{s}^{(N)} - \bar{s}]. \quad (7)$$

In the meantime, the ensemble of measurements is obtained (in the same way as $\mathbf{S}_{m,0}$, i.e. by sampling from the prescribed distribution of measured state variables)

$$\mathbf{S}_{m,1} = [\mathbf{s}_{m,1}^{(1)}, \mathbf{s}_{m,1}^{(2)}, \dots, \mathbf{s}_{m,1}^{(n)}, \dots, \mathbf{s}_{f,1}^{(N-1)}, \mathbf{s}_{m,1}^{(N)}], \quad (8)$$

and the measurement covariance matrix is evaluated by applying \mathcal{C} on $\mathbf{S}_{m,1}$

$$\mathbf{R}_1 = \mathcal{C}(\mathbf{S}_{m,1}). \quad (9)$$

Finally, the analysis step is completed by combining the forecast and measurement as

$$\mathbf{S}_{a,1} = \mathbf{S}_{f,1} + \mathbf{K}_1 (\mathbf{S}_{m,1} - \mathbf{H} \mathbf{S}_{f,1}), \quad (10)$$

where

$$\mathbf{K}_j = \mathbf{P}_{f,j} \mathbf{H}^T \left(\mathbf{H} \mathbf{P}_{f,j} \mathbf{H}^T + \mathbf{R}_j \right)^{-1} \quad (11)$$

is the Kalman gain (with $j = 1$ at the current step). \mathbf{H} is the mapping operator from the model space to the measurement space. Afterwards, both the forecast and analysis steps are repeated for all future time instants $t = t_2, t_3, \dots$, until certain criteria are satisfied (e.g. reaching the desired forecast time t_{\max}).

2.2 | EnKF-FCNN coupled algorithm

We consider a relatively small ensemble size \mathfrak{N} , with which the analysis results (specifically analysis mean $\bar{s}_{a,j}^{\mathfrak{N}}$) while are better than the forecasts, but still show considerable deviations from the truth $s_{t,j}$. Our goal is to utilize FCNN to build a function with the output being a correction term $\Delta s_{a,j}$ as shown in Fig. 2, and the final amended analysis mean given by the EnKF-FCNN algorithm $\bar{s}_{a,j}^{\mathfrak{N}} \leftarrow \bar{s}_{a,j}^{\mathfrak{N}} + \Delta s_{a,j}$ represents a more accurate approximation of $s_{t,j}$. Given that the truth is usually unknown in practical applications, the analysis mean $\bar{s}_{a,j}^{\mathcal{N}}$ given by a relatively large ensemble size \mathcal{N} ($\gg \mathfrak{N}$) is assumed to be a precise surrogate. Therefore, the correction term, namely the output of FCNN, is defined as

$$\Delta s_{a,j} = \bar{s}_{a,j}^{\mathcal{N}} - \bar{s}_{a,j}^{\mathfrak{N}}. \quad (12)$$

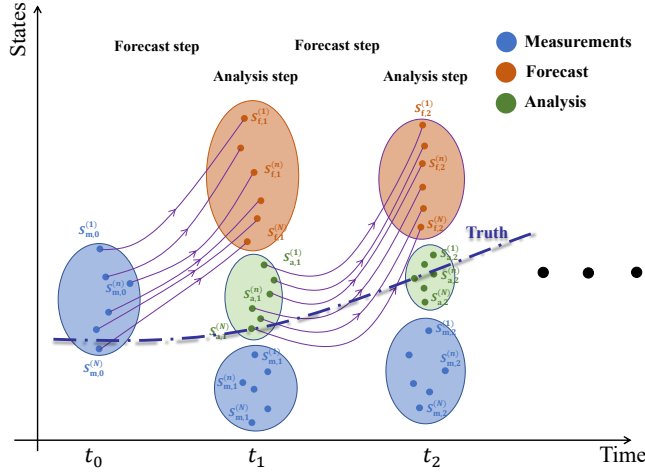


FIGURE 1 Schematic illustration of EnKF (reproduced with modifications from [4]). The size of ellipses represents the level of uncertainty. We use the notation $s_{*,j}^{(n)}$ to represent the n_{th} ($n = 1, 2, \dots, N$) ensemble member state at time $t = t_j$, $j = 0, 1, 2, \dots$, with $*$ = m, f, a for measurement, forecast, and analysis.

In addition, the input variables of the proposed FCNN-based function include $S_{a,j}^{\mathfrak{N}}$, $\bar{s}_{m,j}$, and $\bar{s}_{a,j-1}$. That is to say, our primary goal is to build a function via FCNN as

$$\Delta s_{a,j} = \mathcal{F}(S_{a,j}^{\mathfrak{N}}, \bar{s}_{m,j}, \bar{s}_{a,j-1}; \theta), \quad (13)$$

where θ represents the parameters. We remark that, although the EnKF formula Eq. (10) only includes the current forecast ensemble and the current observations (i.e., the previous state is not explicitly considered), its derivation depends on the flow dependence assumption, namely the Markov chain assumption. Therefore, $\bar{s}_{a,j-1}$ is included as one input to consider the influence of the immediately preceding state.

With the correction term $\Delta s_{a,j}$ given by Eq. (13), each ensemble member is updated as

$$s_{a,j}^{(n)} \leftarrow s_{a,j}^{(n)} + \Delta s_{a,j}, \quad n = 1, 2, \dots, \mathfrak{N}, \quad (14)$$

before performing the next forecast step. Finally, a pseudocode for the complete EnKF-FCNN coupled algorithm is shown in Algorithm 1.

3 | NUMERICAL EXPERIMENTS AND RESULTS

In this study, we perform a set of numerical experiments to demonstrate the feasibility of the proposed EnKF-FCNN coupled algorithm by applying it to the simulations of Lorenz systems [21, 22] and the evolution of nonlinear ocean wave fields. Featured with the chaotic nature, the Lorenz systems are classic “toy” problems in the field of data assimilation; specifically, both Lorenz-63 and Lorenz-96 are tested in this study. In addition, the evolution of nonlinear ocean wave fields has also been shown to be highly sensitive to the model input and parameters, i.e. a small deviation,

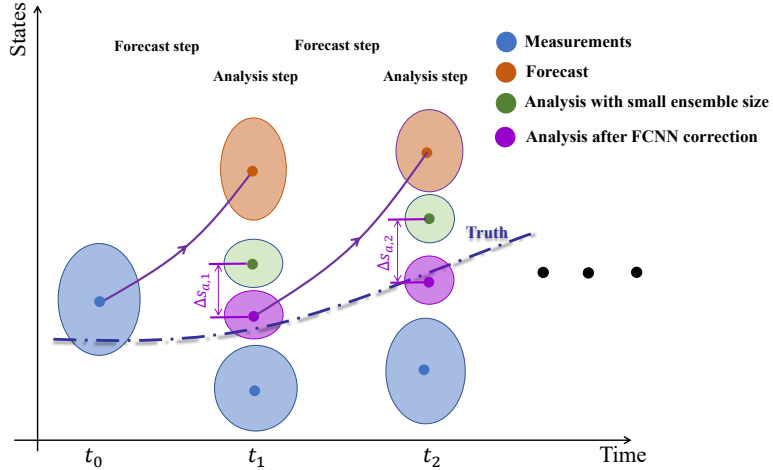


FIGURE 2 Schematic illustration of the EnKF-FCNN coupled algorithm. For the purpose of brevity, only the ensemble mean is shown, omitting individual members.

say, of initial conditions and physical parameters could induce significant forecast errors. Recent studies have shown that DA methods can be conveniently applied to realize the high-accuracy nonlinear wave field simulation [4, 5, 23], which while depends on the relatively large ensemble size ($\sim O(10^2)$), ad-hoc operations (covariance inflation and localization), or both. Here we adopt the Pseudospectral-Fourier-Legendre (PFL) wave model to simulate the nonlinear wave field evolution and evaluate the EnKF-FCNN algorithm by extending the EnKF-PFL computational framework developed in [23].

3.1 | Lorenz-63 and Lorenz-96 systems

In this study, we first perform a set of numerical experiments based on the Lorenz-63 and Lorenz-96 systems. The Lorenz-63 system is expressed as

$$\frac{d\chi}{dt} = \sigma(v - \chi), \quad (15)$$

$$\frac{dv}{dt} = \chi(\rho - \zeta) - v, \quad (16)$$

$$\frac{d\zeta}{dt} = \chi v - \beta\zeta, \quad (17)$$

where χ , v , and ζ represent the system states. σ , ρ , and β are the model parameters, which are set to 10, 28, and $8/3$, respectively, in this study. With a higher dimension than Lorenz-63, Lorenz-96 system is formulated as

$$\frac{d\chi^{(i)}}{dt} = (\chi^{(i+1)} - \chi^{(i-2)})\chi^{(i-1)} - \chi^{(i)} + F, i = 1, 2 \dots L, \quad (18)$$

Algorithm 1 Algorithm for the EnKF-FCNN coupled method

```

1: Input:  $S_{m,0}^{\mathfrak{N}}$  (initial conditions);  $\mathcal{F}$  (pretrained function)
2: Begin:
3: initialize:
4:  $t = t_0, j = 0, S_{a,0}^{\mathfrak{N}} = S_{m,0}^{\mathfrak{N}}$ 
5: time loop:
6:   while  $t \leq t_{\max}$  do
7:      $S_{f,j+1}^{\mathfrak{N}} = \mathcal{M}_{j+1;j}(S_{a,j}^{\mathfrak{N}})$ 
8:     Calculate  $S_{a,j+1}^{\mathfrak{N}}$  with (10)
9:     Calculate  $\Delta s_{a,j+1}$  with (13)
10:    Update  $S_{a,j+1}^{\mathfrak{N}}$  with  $s_{a,j+1}^{(n)} \leftarrow s_{a,j+1}^{(n)} + \Delta s_{a,j+1}, n = 1, 2 \dots \mathfrak{N}$ 
11:    Output  $\bar{s}_{a,j}^{\mathfrak{N}}$  (corrected ensemble mean)
12:     $j \leftarrow j + 1; t \leftarrow t_j$ 
13:  end
14: end

```

where $\chi^{(i)}$ represents the i – th state variable with L variables in total. In this study, we consider a case of $L = 10$, and the periodic boundary condition is applied. F is a constant external forcing term, which is set to be $F = 8$. In addition, both Lorenz-63 and Lorenz-96 systems are solved using a first-order forward difference scheme with a time step $\Delta t = 0.01$.

At the analysis step, the measurements are needed, which can approximate the truth yet with some noise. In this study, we first produce the (synthetic) truth $s_{t,j}$ by running a set of reference simulations with presumed exact initial conditions. Then an error δ randomly sampled from a given distribution is superposed on top of $s_{t,j}$ to produce $\bar{s}_{m,j}$, i.e.

$$\bar{s}_{m,j} = s_{t,j} + \delta. \quad (19)$$

Here we assume that δ follows a normal distribution with zero mean and covariance matrix Σ . Particularly, we set $\Sigma = A\mathbf{I}$, with A being the magnitude and \mathbf{I} being an identity matrix. Finally, the observation ensemble members are generated as

$$s_{m,j}^{(n)} = \bar{s}_{m,j} + \delta_e^{(n)}, \quad (20)$$

where $\delta_e^{(n)}$ is also a random error and assumed to follow the same distribution as δ . For the Lorenz-63 system, we assume that the measurements for all three variables are available; while for the Lorenz-96 system, we consider that the observations are only available for 5 variables, i.e. $\chi^{(i)}$ with $i = \{1, 3, 5, 7, 9\}$. In addition, the data assimilation interval is set to be $T_{\text{DA}} = 8\Delta t$ and $T_{\text{DA}} = 5\Delta t$ for Lorenz-63 and Lorenz-96, respectively. Here we remark that a relatively small data assimilation interval is adopted for Lorenz-96 given its more pronounced chaotic behavior.

To generate the datasets needed to build FCNN, we consider $K = 100$ uniformly distributed initial conditions for both Lorenz-63 and Lorenz-96 with the train/test split ratio being 80 – 20. Then the traditional EnKF-based simulations (i.e. without FCNN) are performed with $\mathcal{N} = 100$ and $\mathfrak{N} = 7$, and the results for a period of $80T_{\text{DA}}$ are adopted as the datasets. Figs. 3-4 show the results for one particular initial condition obtained with $\mathcal{N} = 100$ and $\mathfrak{N} = 7$, as

well as the truth, for Lorenz-63 and Lorenz-96, respectively. For the Lorenz-63 system, it can be found that when using $\mathcal{N} = 100$, the analysis results are always closely following the truth. In contrast, when reducing the ensemble size to $\mathfrak{N} = 7$, significant discrepancies between the analysis results and truth can be observed. The overall trend is similar for the Lorenz-96 system, as shown in Fig. 4. Therefore, it is reasonable to define the correction term in Eq. (12), i.e. the output of FCNN, with $\mathcal{N} = 100$ and $\mathfrak{N} = 7$.

To build FCNNs predicting the correction terms for Lorenz-63 and Lorenz-96, we use the rectified linear unit (ReLU) as the activation function and mean squared error (MSE) as the loss function, and the detailed configuration of other hyperparameters is shown in Tab. 1.

TABLE 1 Hyperparameters of FCNN for different numerical simulations

	Lorenz-63	Lorenz-96	2D Wave	3D Wave
size of input layer	27	115	5384	21514
size of hidden layer 1	60	200	10000	8000
size of hidden layer 2	15	100	2500	4000
size of hidden layer 3	7	40	500	2000
size of output layer	3	10	256	1024

TABLE 2 Computational time for different calculations on a single Intel Core Ultra 9 CPU

Cases	A single simulation for T_{DA} (s)	FCNN function (s)
Lorenz-63	6.15e-4	7.68e-5
Lorenz-96	2.62e-3	2.91e-4
2D wave	4.69e-1	8.62e-4
3D wave	2.72	1.90e-3

Figures 5-6 present the results of $\bar{s}_a^{\mathfrak{N}}$ produced by the EnKF-FCNN algorithm in comparison with $\bar{s}_a^{\mathcal{N}}$ given by the traditional EnKF, for Lorenz-63 and Lorenz-96, respectively. It can be found that for Lorenz-63, with the FCNN-based correction term, $\bar{s}_a^{\mathfrak{N}}$ can always closely follow $\bar{s}_a^{\mathcal{N}}$, which indicates that the proposed EnKF-FCNN algorithm can effectively ameliorate the filter divergence issue suffered by the traditional EnKF in the scenario with a limited ensemble size. In terms of the Lorenz-96 system, the proposed EnKF-FCNN can also remedy the analysis results given by \mathfrak{N} substantially, although the overall performance is inferior to that in the case with Lorenz-63 system to some extent. This degraded performance is likely due to the Lorenz-96 system's higher nonlinearity and dimensionality, which may lead to a more complex relationship between the input and output. Although it is possible to address this issue through hyperparameter optimization, the objective and scope of this paper are specifically to demonstrate the potential of machine learning methods to aid DA. Therefore, a comprehensive analysis of hyperparameter impacts is not undertaken here.

In addition, an error metric is defined to quantitatively evaluate the overall performance of the proposed EnKF-

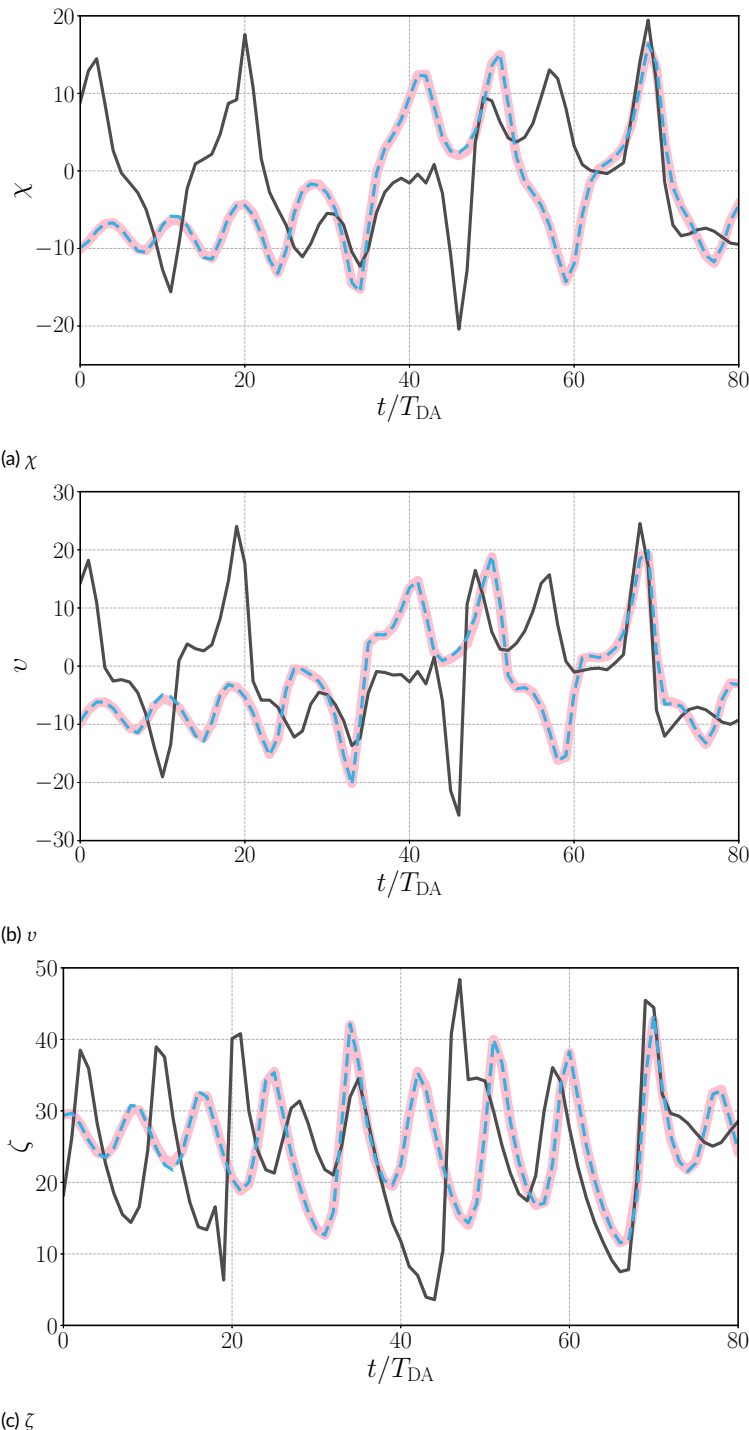


FIGURE 3 Analysis results obtained with the traditional EnKF using $\mathcal{N} = 100$ (—) and $\mathfrak{N} = 7$ (—), as well as the true solution (— - -), for Lorenz-63

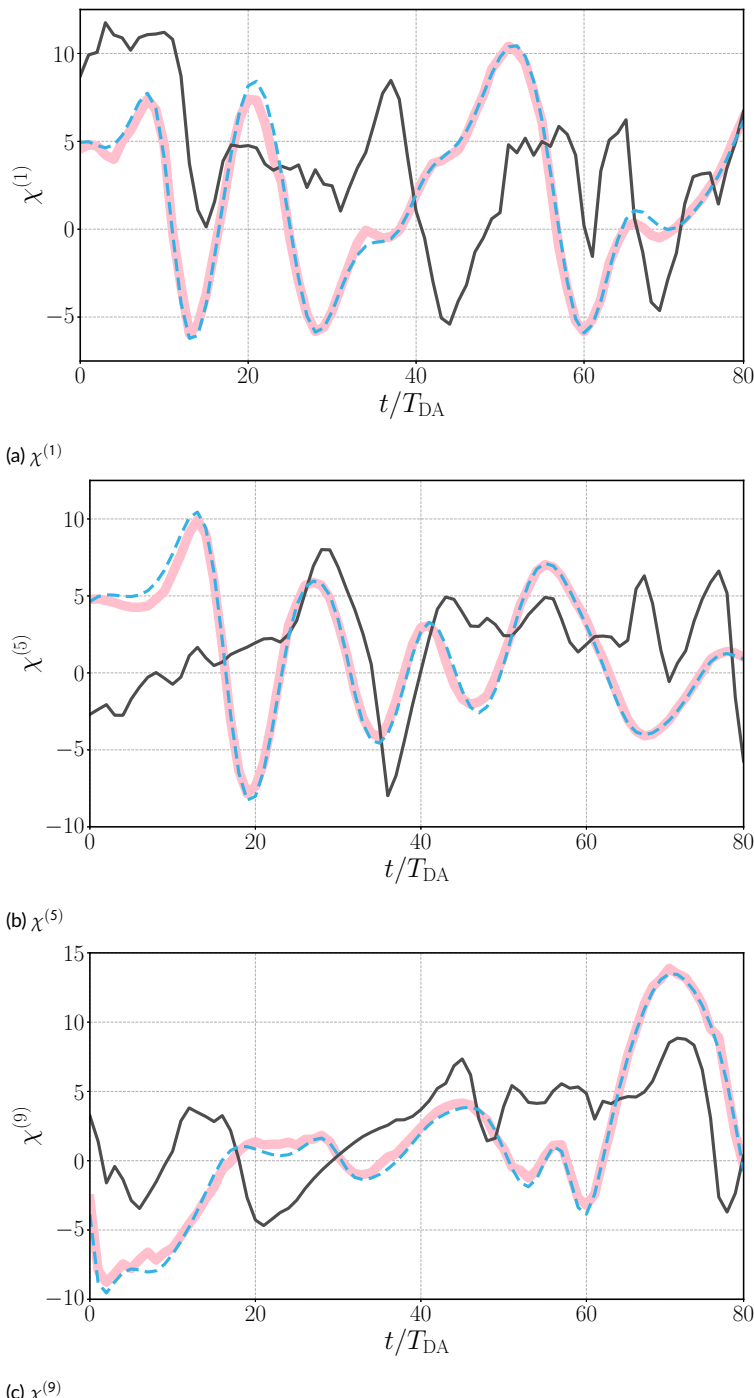


FIGURE 4 Analysis results obtained with the traditional EnKF using $\mathcal{N} = 100$ (—) and $\mathfrak{N} = 7$ (—), as well as the true solution (— - -), for Lorenz-96

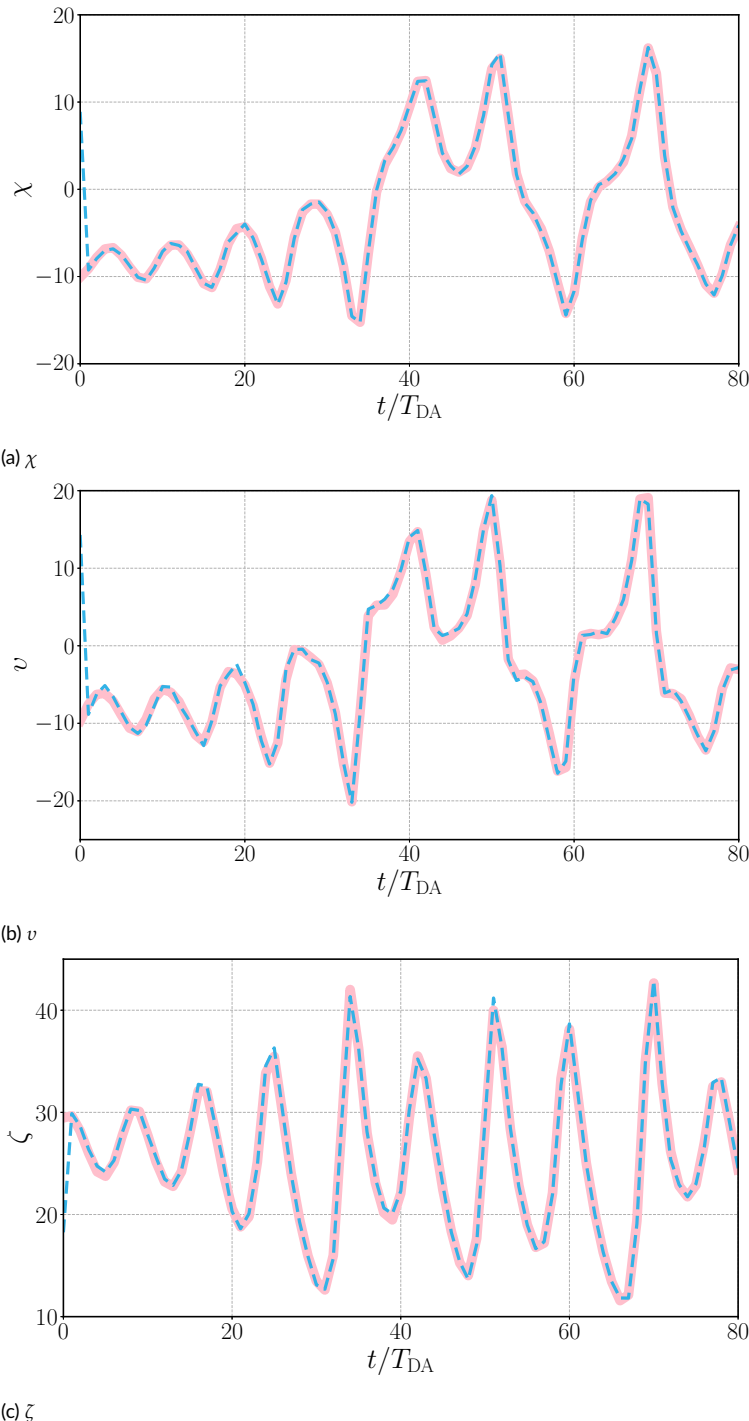


FIGURE 5 Analysis results given by the EnKF-FCNN algorithm with $\mathcal{N} = 7$ (---) and traditional EnKF with $\mathcal{N} = 100$ (—) for Lorenz-63

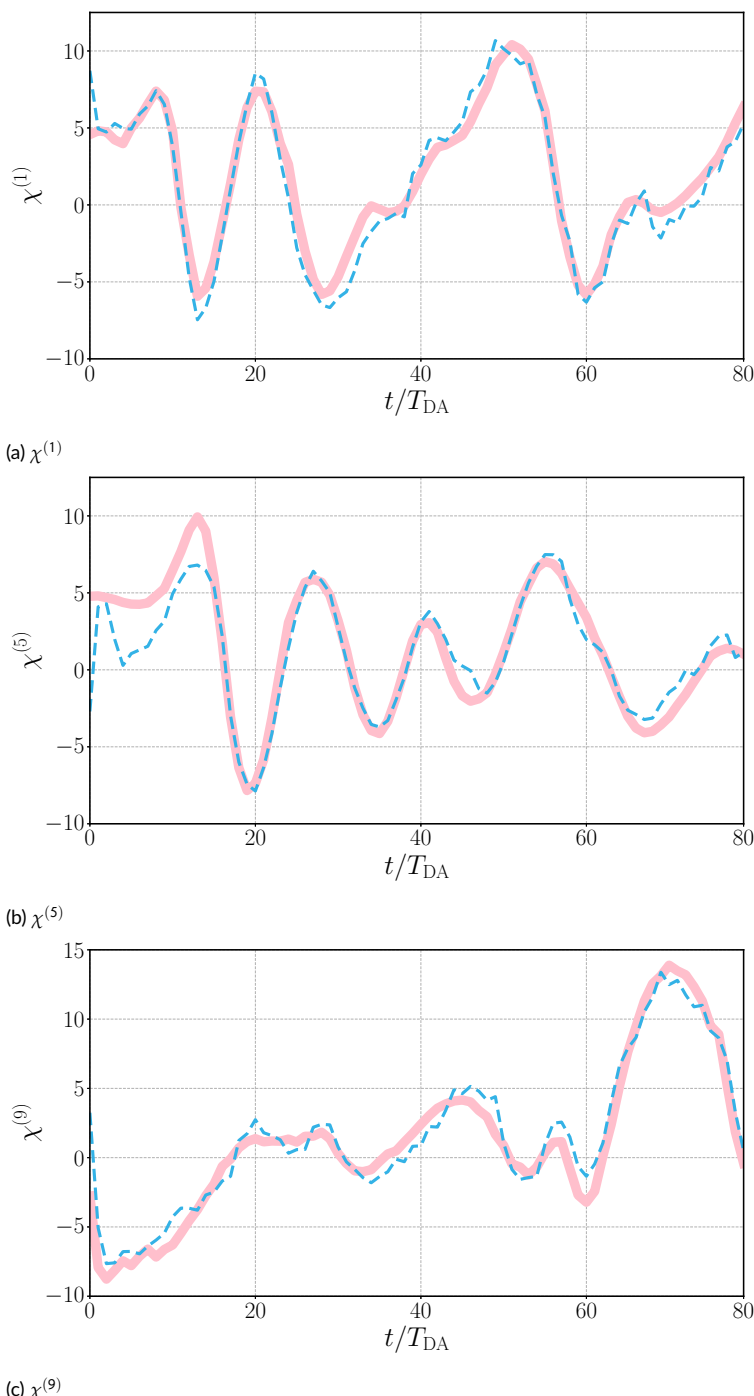


FIGURE 6 Analysis results given by the EnKF-FCNN algorithm with $\mathfrak{N} = 7$ (---) and traditional EnKF with $\mathcal{N} = 100$ (—) for Lorenz-96

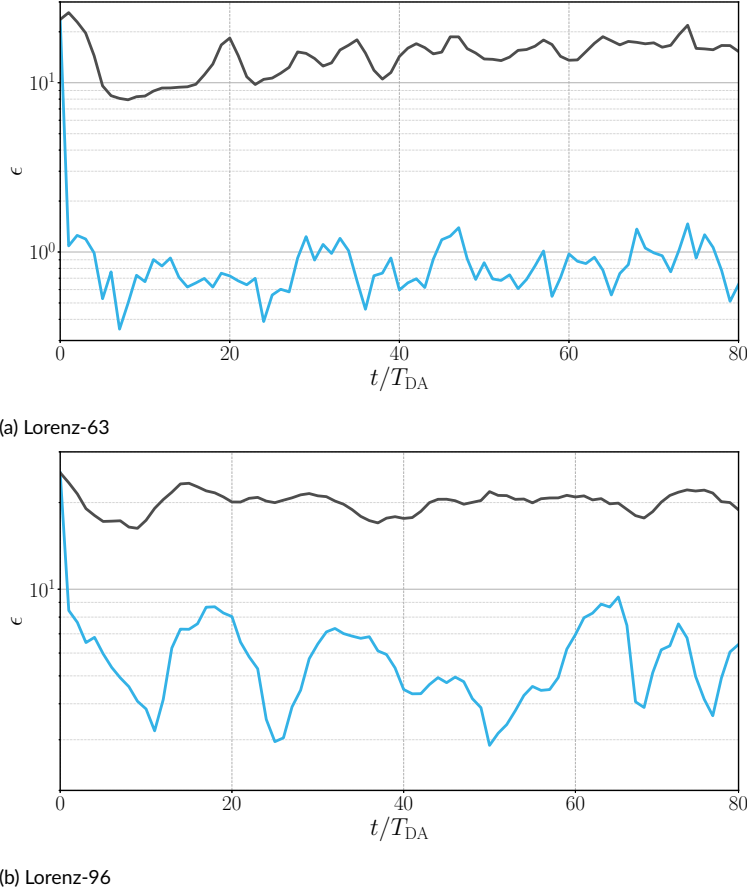


FIGURE 7 $\epsilon(t)$ of traditional EnKF (—) and EnKF-FCNN (—) with $\mathfrak{N} = 7$ for Lorenz systems

FCNN algorithm

$$\epsilon(t_j) = \frac{1}{K_t} \sum_{k=1}^{K_t} \|\bar{s}_{u,j}^{\mathfrak{N}} - \bar{s}_{u,j}^{\mathcal{N}}\|_2^{(k)}, \quad (21)$$

where K_t is the number of initial conditions in the test dataset, with k being the index. Here we evaluate $\epsilon(t)$ using both the traditional EnKF and EnKF-FCNN with the same limited ensemble size $\mathfrak{N} = 7$, for which the results are shown in Fig 7. It can be found that for Lorenz-63, after applying the ML-based correction, $\epsilon(t)$ is reduced by one order of magnitude. For Lorenz-96, the improvement is less significant, but still with the error reduced by a factor of approximately 3.

Finally, we evaluate the computational time of the FCNN function, as compared to that of performing a single simulation for T_{DA} . As shown in Tab. 2, for both Lorenz-63 and Lorenz-96, the computational time consumed by implementing the FCNN-based correction is approximately one order of magnitude lower than running a single simulation for T_{DA} , which means that the additional computational cost induced by the former is practically negligible.

3.2 | Nonlinear ocean wave simulation

To further demonstrate the performance of the developed EnKF-FCNN algorithm, we apply it on the nonlinear ocean wave simulation with the PFL method.

The governing equations for the ocean wave field are formulated as

$$\frac{\partial \eta(\mathbf{x}, t)}{\partial t} + \frac{\partial \psi(\mathbf{x}, t)}{\partial \mathbf{x}} \cdot \frac{\partial \eta(\mathbf{x}, t)}{\partial \mathbf{x}} - \left[1 + \frac{\partial \eta(\mathbf{x}, t)}{\partial \mathbf{x}} \cdot \frac{\partial \eta(\mathbf{x}, t)}{\partial \mathbf{x}} \right] w(\mathbf{x}, t) = 0 \quad (22)$$

$$\frac{\partial \psi(\mathbf{x}, t)}{\partial t} + \frac{1}{2} \frac{\partial \psi(\mathbf{x}, t)}{\partial \mathbf{x}} \cdot \frac{\partial \psi(\mathbf{x}, t)}{\partial \mathbf{x}} + g\eta(\mathbf{x}, t) - \frac{1}{2} \left[1 + \frac{\partial \eta(\mathbf{x}, t)}{\partial \mathbf{x}} \cdot \frac{\partial \eta(\mathbf{x}, t)}{\partial \mathbf{x}} \right] w(\mathbf{x}, t)^2 = 0, \quad (23)$$

$$\nabla^2 \phi = 0, \quad (24)$$

where $\eta(\mathbf{x}, t)$ is the free surface elevation, ϕ is the velocity potential, $\psi = \phi|_{z=\eta}$ is the velocity potential on the free surface, $w = (\partial \phi / \partial z)|_{z=\eta}$ is the surface vertical velocity, and g is the gravity acceleration. The key procedure in PFL is to solve Eq. (24) by assuming an artificial boundary condition at one particular depth, with details included in multiple papers such as [24, 25]. In particular, we directly adopt the PFL-EnKF framework developed by Wang et al. [23] as the basis to test the performance of the EnKF-FCNN coupled algorithm. Both two-dimensional (2D) and three-dimensional (3D) irregular wave fields are considered in this study, with the same case configurations in [23]. To produce the dataset, we first randomly generate 100 initial conditions from a JONSWAP spectrum with the peak steepness $Ak_p = 0.12$ and an enhance factor $\gamma = 3.3$, and then run the original PFL-EnKF simulations with $\mathcal{N} = 100$ and $\mathfrak{N} = 20$. Fig. 8 presents the time histories of surface elevation at three locations ($x/\mathcal{L} = 0.15, 0.50$, and 0.85 with \mathcal{L} being the simulation domain length) of the 2D wave field obtained with the two ensemble sizes, as well as the truth, for one particular initial condition. It can be found that, with $\mathcal{N} = 100$, the PFL-EnKF framework can give a good approximation of the truth. In contrast, when using $\mathfrak{N} = 20$, the analysis results differ significantly from the truth, especially at the wave crests and troughs. A similar trend can be observed for the 3D wave field, as shown in Fig. 9. To build the FCNN, we use the same activation and loss functions as the Lorenz problems, with all other hyperparameters shown in Tab. 1.

Figures 10-11 show the analysis results $\bar{\eta}_a^{\mathfrak{N}}$ given by the EnKF-FCNN algorithm for both 2D and 3D wave fields, respectively, in comparison with $\bar{\eta}_a^{\mathcal{N}}$ produced by the traditional EnKF. It can be found that, for both 2D and 3D wave fields, the EnKF-FCNN algorithm with $\mathfrak{N} = 20$ can always demonstrate comparable performance to the traditional EnKF with $\mathcal{N} = 100$, which again confirms the EnKF-FCNN's capability of overcoming the filter divergence issue induced by the limited ensemble size. Fig. 12 compares the results of $\epsilon(t)$ obtained with the traditional EnKF and EnKF-FCNN, in which the ensemble size is always $\mathfrak{N} = 20$, for both 2D and 3D wave fields. It can be observed that, by applying the FCNN correction at each analysis step, $\epsilon(t)$ can be consistently reduced by more than 50% for both 2D and 3D wave fields. Similar to the Lorenz systems, we also compare the computational time induced by running the FCNN function with that of running a single simulation for T_{DA} , with the former approximately three orders of magnitude lower than the latter as shown in Tab. 2, which again confirms the computational efficiency of the proposed EnKF-FCNN algorithm.

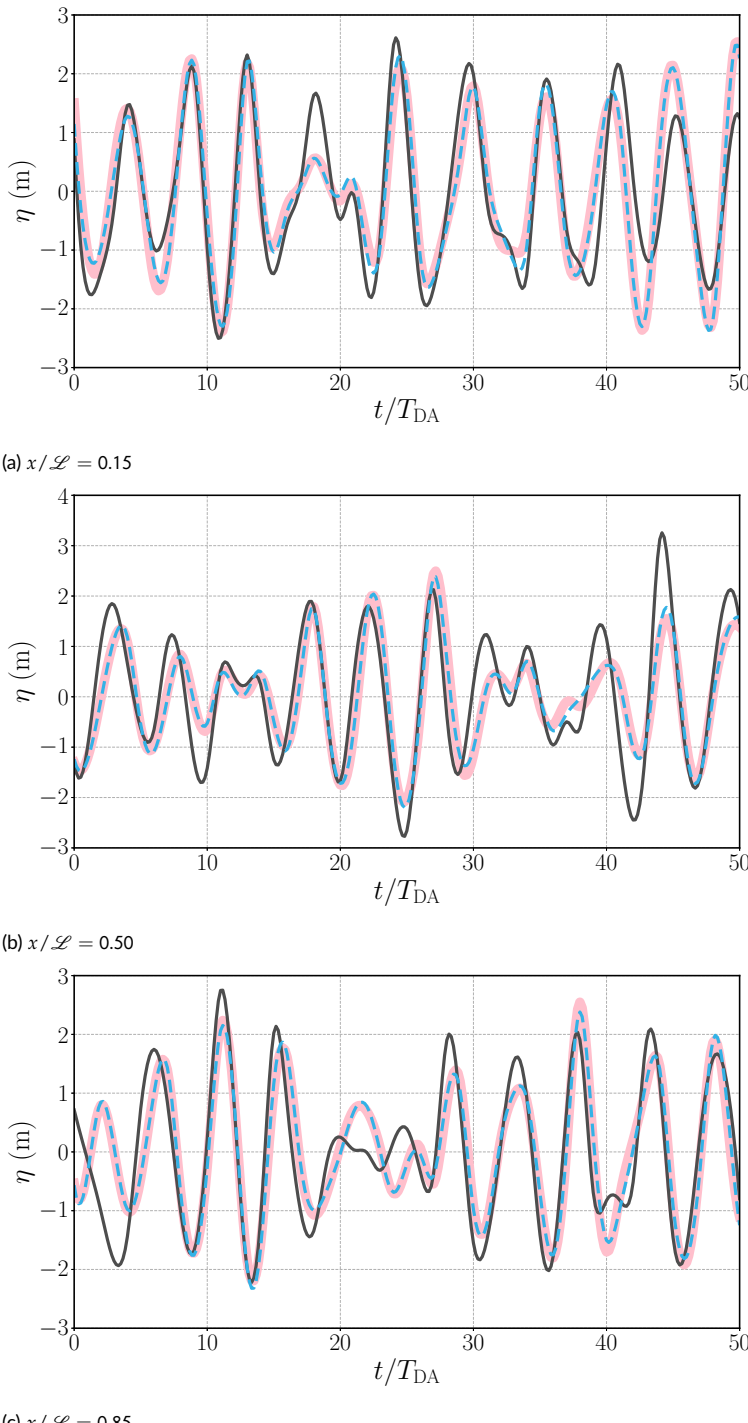


FIGURE 8 Analysis results of $\eta(t)$ obtained with the traditional EnKF using $\mathcal{N} = 100$ (—) and $\mathfrak{N} = 20$ (—), as well as the true solution (—), for the 2D wave field

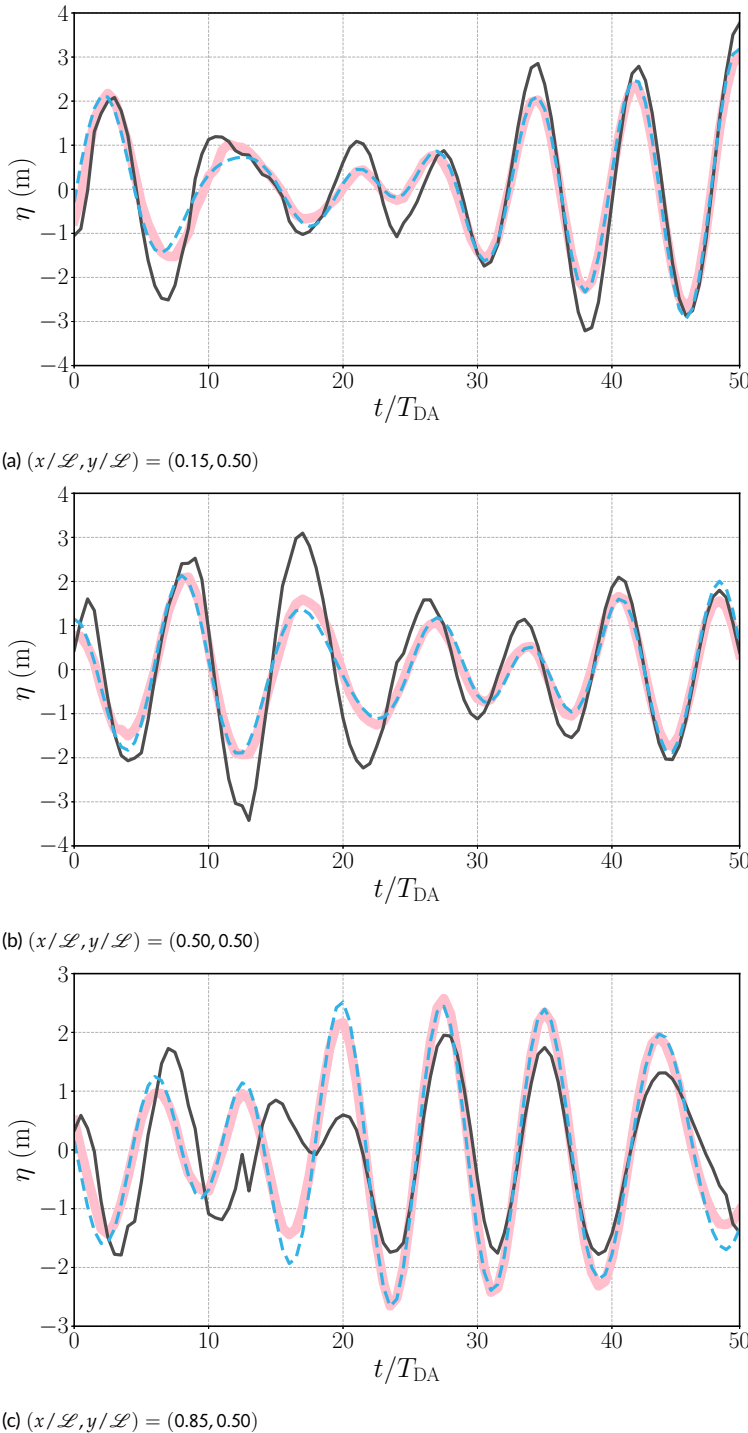


FIGURE 9 Analysis results of $\eta(t)$ obtained with the traditional EnKF using $\mathcal{N} = 100$ (—) and $\mathfrak{N} = 20$ (—), as well as the true solution (---), for the 3D wave field

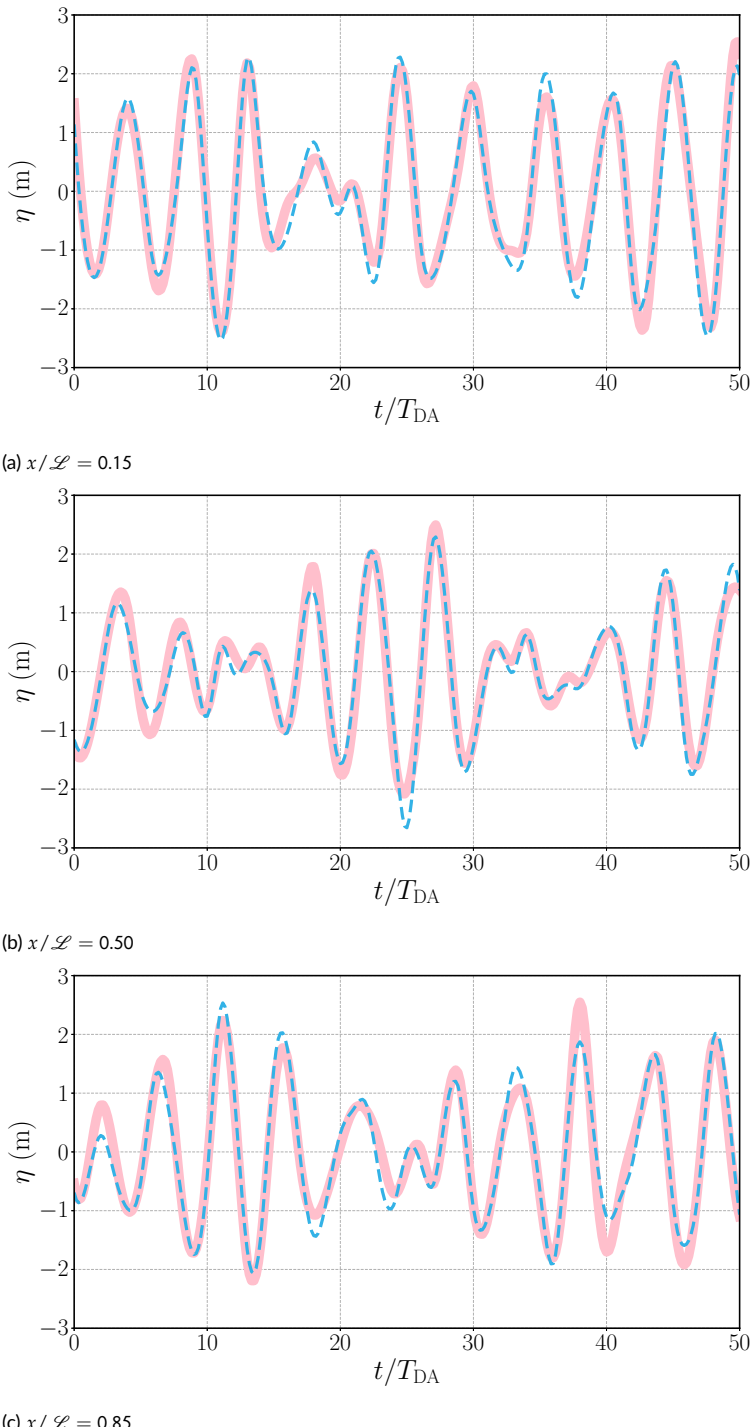


FIGURE 10 Analysis results of $\eta(t)$ given by the EnKF-FCNN algorithm with $\mathfrak{R} = 20$ (---) and traditional EnKF with $\mathcal{N} = 100$ (—) for the 2D wave field

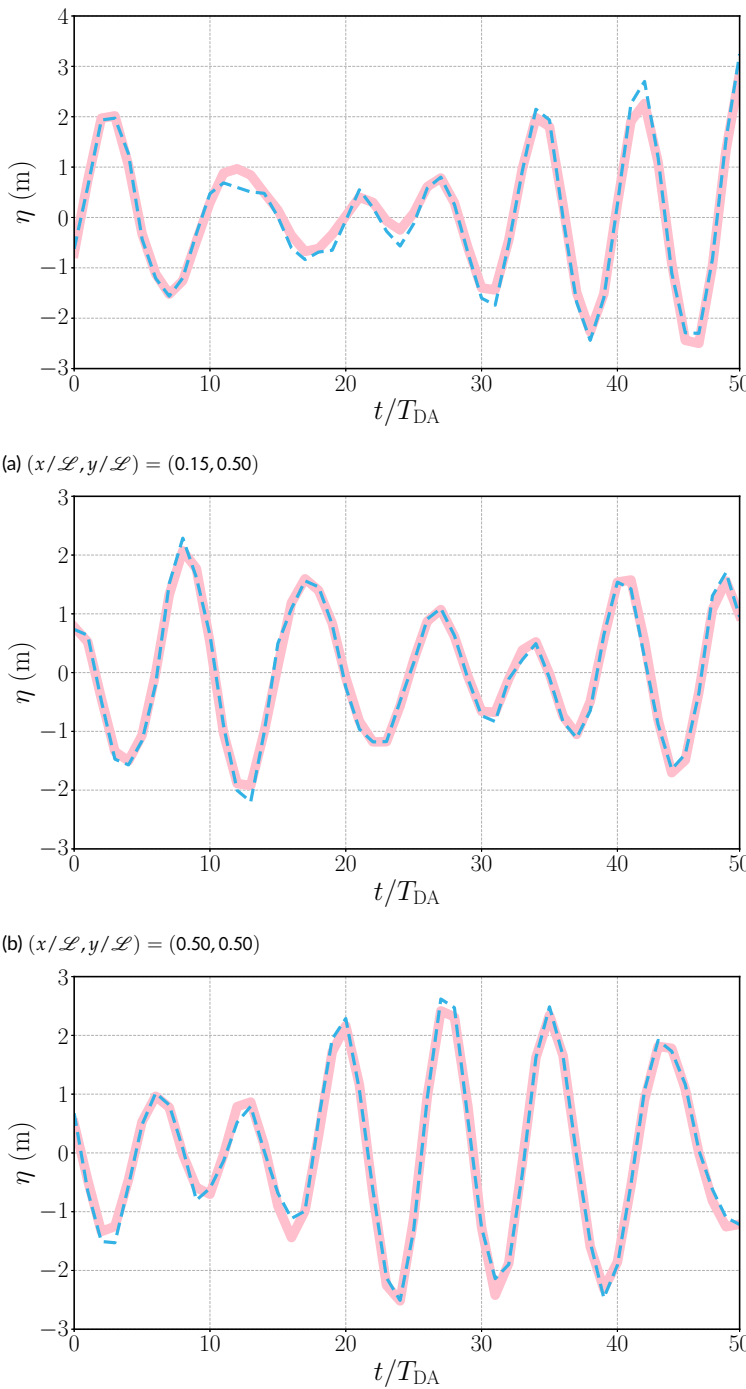


FIGURE 11 Analysis results of $\eta(t)$ given by the EnKF-FCNN algorithm with $\mathfrak{R} = 20$ (---) and traditional EnKF with $\mathcal{N} = 100$ (—) for the 3D wave field

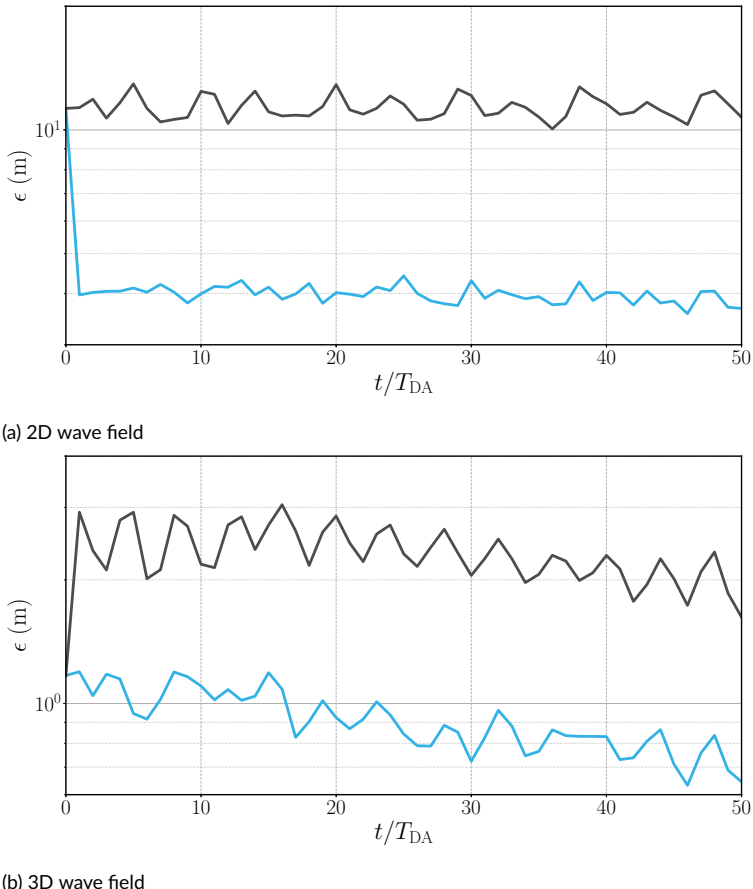


FIGURE 12 $\epsilon(t)$ of traditional EnKF (—) and EnKF-FCNN (—) with $\mathfrak{N} = 20$ for wave fields

4 | CONCLUSION

In this study, we develop a novel EnKF-FCNN coupled algorithm, which aims at improving the robustness of the traditional EnKF method in the scenario of a limited ensemble size. The developed EnKF-FCNN algorithm is validated and tested through a set of numerical experiments based on the numerical simulations of Lorenz systems and nonlinear ocean wave fields. As indicated by the numerical results, the proposed EnKF-FCNN approach enhances the analysis accuracy significantly when working with limited ensemble sizes while introducing minimal additional computational cost. In addition, the developed EnKF-FCNN method can be easily adapted to diverse practical applications, by coupling with different numerical models and substituting the EnKF with other ensemble-based DA methods.

Acknowledgements

This research is financially supported by the National Natural Science Foundation of China (52301336), the Science and Technology Development Fund of Macau S.A.R. (0048/2025/ITP1), the University of Macau (SRG2025-00004-FST), and Zhejiang Provincial Natural Science Foundation of China (LQN25E090004).

Data Availability

The data that support the findings of this study are available from the corresponding author upon reasonable request.

Conflict of interest

The authors have no conflicts of interest to declare.

references

- [1] Carrassi A, Bocquet M, Bertino L, Evensen G. Data assimilation in the geosciences: An overview of methods, issues, and perspectives. *WIREs Climate Change*, 9, e535; 2018.
- [2] Bocquet M, Elbern H, Eskes H, Hirtl M, Žabkar R, Carmichael G, et al. Data assimilation in atmospheric chemistry models: current status and future prospects for coupled chemistry meteorology models. *Atmospheric chemistry and physics* 2015;15(10):5325–5358.
- [3] Eyre J, Bell W, Cotton J, English S, Forsythe M, Healy S, et al. Assimilation of satellite data in numerical weather prediction. Part II: Recent years. *Quarterly Journal of the Royal Meteorological Society* 2022;148(743):521–556.
- [4] Wang G, Pan Y. Phase-resolved ocean wave forecast with ensemble-based data assimilation. *Journal of Fluid Mechanics* 2021;918:A19.
- [5] Wang G, Zhang J, Ma Y, Zhang Q, Li Z, Pan Y. Phase-resolved ocean wave forecast with simultaneous current estimation through data assimilation. *Journal of Fluid Mechanics* 2022;949:A31.
- [6] Martin MJ, Hoteit I, Bertino L, Moore AM. Data assimilation schemes for ocean forecasting: state of the art. *State of the Planet* 2025;5:1–12.
- [7] Li X, Liu F, Ma C, Hou J, Zheng D, Ma H, et al. Land data assimilation: Harmonizing theory and data in land surface process studies. *Reviews of Geophysics* 2024;62(1):e2022RG000801.

[8] Felsberg A, De Lannoy GJ, Girotto M, Poesen J, Reichle RH, Stanley T. Global soil water estimates as landslide predictor: the effectiveness of SMOS, SMAP, and GRACE observations, land surface simulations, and data assimilation. *Journal of Hydrometeorology* 2021;22(5):1065–1084.

[9] Evensen G. Sequential data assimilation with a nonlinear quasi-geostrophic model using Monte Carlo methods to forecast error statistics. *Journal of Geophysical Research: Oceans* 1994;99(C5):10143–10162.

[10] Evensen G. The ensemble Kalman filter: Theoretical formulation and practical implementation. *Ocean dynamics* 2003;53:343–367.

[11] Petrie RE, Dance SL. Ensemble-based data assimilation and the localisation problem. *Weather* 2010;65(3):65–69.

[12] Whitaker JS, Hamill TM. Evaluating methods to account for system errors in ensemble data assimilation. *Monthly Weather Review* 2012;140(9):3078–3089.

[13] Buehner M, Charron M. Spectral and spatial localization of background-error correlations for data assimilation. *Quarterly Journal of the Royal Meteorological Society: A journal of the atmospheric sciences, applied meteorology and physical oceanography* 2007;133(624):615–630.

[14] Kang JS, Kalnay E, Miyoshi T, Liu J, Fung I. Estimation of surface carbon fluxes with an advanced data assimilation methodology. *Journal of Geophysical Research: Atmospheres* 2012;117(D24).

[15] Evensen G, Vossepoel FC, Van Leeuwen PJ. Data assimilation fundamentals: A unified formulation of the state and parameter estimation problem. Springer Nature; 2022.

[16] Choi B, Lee Y. Sampling error mitigation through spectrum smoothing: First experiments with ensemble transform Kalman filters and Lorenz models. *Physica D: Nonlinear Phenomena* 2025;472:134436.

[17] Brajard J, Carrassi A, Bocquet M, Bertino L. Combining data assimilation and machine learning to emulate a dynamical model from sparse and noisy observations: A case study with the Lorenz 96 model. *Journal of computational science* 2020;44:101171.

[18] Sun H, Lei L, Liu Z, Ning L, Tan ZM. An online paleoclimate data assimilation with a deep learning-based network. *Journal of Advances in Modeling Earth Systems* 2025;17(6):e2024MS004675.

[19] Arcucci R, Zhu J, Hu S, Guo YK. Deep data assimilation: integrating deep learning with data assimilation. *Applied Sciences* 2021;11(3):1114.

[20] Wu P, Chang X, Yuan W, Sun J, Zhang W, Arcucci R, et al. Fast data assimilation (FDA): Data assimilation by machine learning for faster optimize model state. *Journal of Computational Science* 2021;51:101323.

[21] Lorenz EN. Deterministic nonperiodic flow. *Journal of atmospheric sciences* 1963;20(2):130–141.

[22] Lorenz EN. Predictability: A problem partly solved. In: Proc. Seminar on predictability, vol. 1 Reading; 1996. p. 1–18.

[23] Wang S, Zhang L, Liu Z, Sun J, Yang X, Wang G. Nonlinear phase-resolved ocean wave simulation with ensemble Kalman filter. *Phys Rev Fluids* 2025 Aug;.

[24] Klahn M, Madsen PA, Fuhrman DR. On the accuracy and applicability of a new implicit Taylor method and the high-order spectral method on steady nonlinear waves. *Proceedings of the Royal Society A* 2020;476(2243):20200436.

[25] Klahn M, Madsen PA, Fuhrman DR. Simulation of three-dimensional nonlinear water waves using a pseudospectral volumetric method with an artificial boundary condition. *International Journal for Numerical Methods in Fluids* 2021;93(6):1843–1870.